

COUPLING FAILURE FOR TORSIONAL FATIGUE: A MULTI-DISCIPLINARY ROOT CAUSE ANALYSIS APPROACH

Valerio Rossi

GE Oil&Gas, Florence, Italy, I-50127,
valerio.rossi@ge.com

Marco Romanelli

GE Oil&Gas, Florence, Italy, I-50127,
marco.romanelli@ge.com

Lorenzo Naldi

GE Oil&Gas, Florence, Italy, I-50127,
lorenzo.naldi@ge.com

Luca Antonelli

GE Oil&Gas, Florence, Italy, I-50127,
luca.antonelli@ge.com

Marco Manetti

GE Oil&Gas, Florence, Italy, I-50127,
marco.manetti@ge.com

Roberto Paolanti

GE Oil&Gas, Florence, Italy, I-50139,
roberto.paolanti@ge.com

ABSTRACT

The successful growth of an EHS culture, focus on equipment availability and reliability, as well as continuous pressure on increased production is causing a higher demand for improvements in Root Cause Analysis (RCA) quality and speed of completion. Root causes investigations need to be driven to a strong level of understanding and resolution to guarantee safe operation, to optimize production and to reduce costs.

RCA processes are many times based on different disciplines to investigate the most challenging failures having the following characteristics:

- *Top Critical: potential impact on safety and production;*
- *First occurrence: no similar cases investigated before;*
- *Lack of information: no operation data and only fragmented information available.*

In these cases only a multi disciplinary approach allows studying various aspects of the failure and validating the results as an overall system solution.

In this paper the authors present a recent study where finite element stress model calculations, metallurgical laboratory analysis (fractography examination, mechanical testing, fracture mechanics), dynamic analysis, fatigue tests and field measurements were used to investigate causes of coupling failure and determinate corrective actions. Results of each study are presented with special focus on comparative analysis and data matching.

1. INTRODUCTION

The authors experienced some cases of minor coupling damages/failures on LNG trains; three of these damages occurred on two lineups in Egypt (see and for layout).

- Jan. 2005: T2 found 7 bolts broken on the coupling HM side (HM flange drive end side);

- May 2006 T2 high-high Vibrations on the Helper Motor: found 5 bolts of the coupling broken (HM flange drive end side).
- Sept. 2007 T1 high-high Helper Motor Vibrations: failure of a spacer bolt (see section “E”);

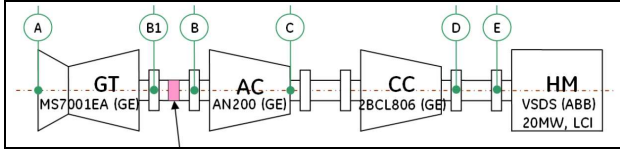


Figure 1: MR TRAIN (T1)

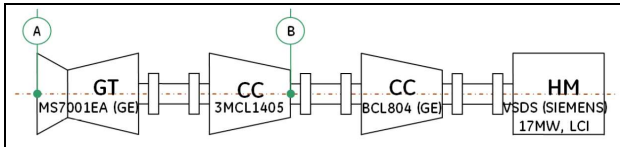


Figure 2: PR + MR TRAIN (T2)

Initially each issue was addressed with a different RCA until a major failure occurred on November 2008. At that time high-high radial vibrations were detected on GT radial probes; a visual inspection of the GT-CC load coupling highlighted a clearly visible crack on the flange radius.

Refer to and for details about damage and location.

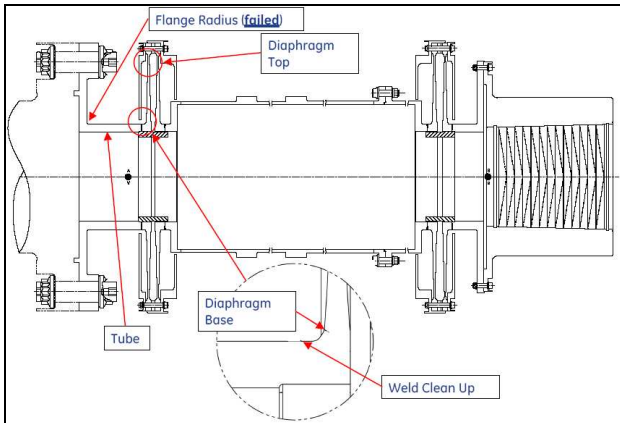


Figure 3: COUPLING DRAWING



Figure 4: DAMAGED COUPLING

A structured RCA process was set up to investigate the root cause in detail and to propose a systematic corrective action plan for the problem.

Different departments were involved in this process:

- MPE: Material and Process Engineering
- Rotordynamic
- Design: Shaft Line Integration
- Testing.

To investigate all the aspects of this issue, the Cause and Effect study focusing on:

- Design:
 - Tube dimensions;
 - Insufficient fillet radius;
- Material:
 - Improper forging fiber cutting;
 - Base material out of specification;
 - Presence of defect;
- Manufacturing handling:
 - Superficial scratch;
- Anti-flail wrong position :
 - Stress generated by a wrong positioning;
- Torsional vibration:
 - Torsional excitation generating resonance and as consequence a cyclic torque greater than 55000 Nm;
- High misalignment:
 - Misalignment greater than allowable.

shows the fishbone associated to the RCA process: the first three aspects are relevant to coupling performance lower than expected; whereas the last ones are relevant to operation conditions more severe than expected.

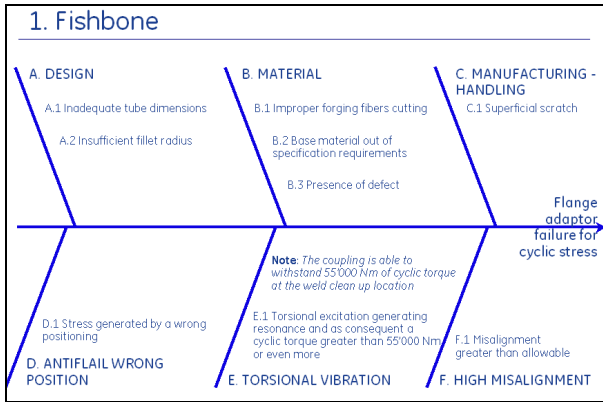


Figure 5: RCA FISHBONE

Although all the potential causes listed in the fishbone were investigated during the RCA process, only a part of them will be reported in this paper that will focus on the causes that resulted determinant for the failure.

This paper presents the results coming from these different analysis, shows data matching and reports how the results coming from the different studies validated each other.

2. FAILURE DESCRIPTION

The root cause analysis has been performed on the gas turbine flexible load coupling in the CC train driven by dual option GT-motor drivers. The coupling design was fabricated from a low alloy steel with 1% of nickel. An image of the broken coupling flange adaptor is showed in .

Looking to the component and the fracture surface, there are clear evidences of a fatigue fracture during service.

To analyze the fracture surface, a characterization with the stereoscope has been done. An image of a cut fracture surface is shown in

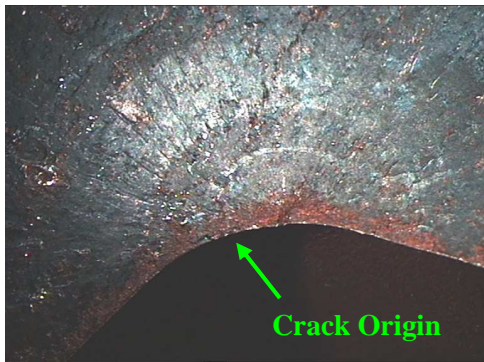


Figure 6: STEREOSCOPIC IMAGE OF THE CRACK ORIGIN ZONE

As can be seen, the fracture surface shows characteristic fatigue path propagation. It is simple to identify the crack initiation zone and the propagation due to fatigue stress. At higher magnification is also possible to identify secondary cracks just below crack origin area. The fracture surface shows different zones, characterized by two different colors, which probably indicates different service condition from the initiation of the crack through the propagation of the flaw to critical size and fracture. Since more detailed investigation of the two zones was required, a higher magnification was called for.

It is very important to note that no defects related to corrosion damage on the surface, subsurface material quality (metallurgical issue) or machining (scratches) on the crack initiation surface were detected and the initial hypothesis was that the defect could have been initiated during fatigue cycles higher than the limits.

Deep analysis has been done using a scanning electron microscope (SEM) that allows analyzing the fracture surface at higher magnification (for this fracture surface, up to 50000x). An image of the crack path grabbed with SEM using secondary electron is shown in

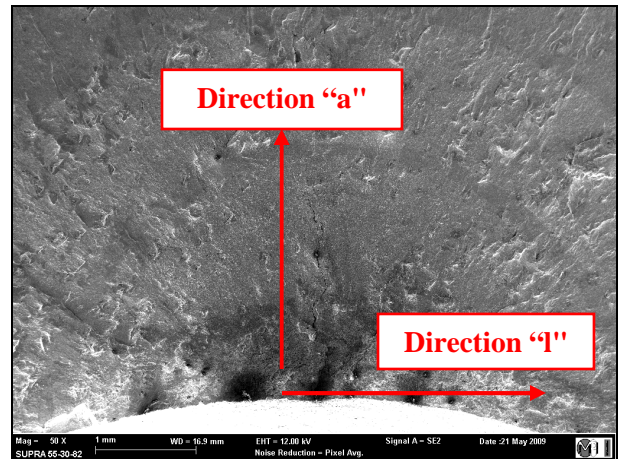


Figure 7: SEM IMAGE OF THE CRACK ORIGIN ZONE

At this magnification, is very simple to identify the different zones and is important to make a photographic documentation.

The principal scope of the SEM analysis is to measure and count the fatigue striations. Following the principal growth direction of the cracks (identified with “a” and “I” starting from crack origin, see ; crack dimensions are ~18 mm in “a” direction and ~35 mm in “I” direction), the fatigue striations per micron have been counted, at different distances from initial crack zone. An example of analyzed zone is shown in **Error! Reference source not found..**

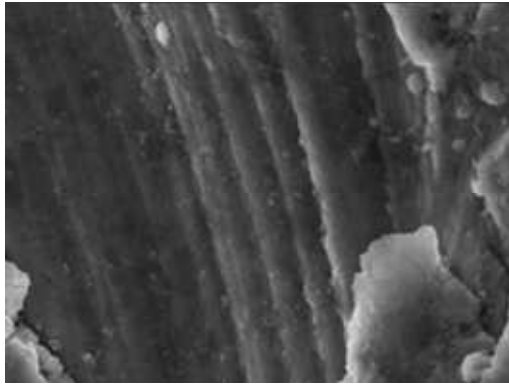


Figure 8: STRIATIONS IN “A” DIRECTION

This is a fundamental phase, because the striations per micron are one of the elements of data necessary for estimating the actual alternating stress cycles acting on the components and for determining the cyclic growth controlling the damage to the coupling.

3. DESIGN VERIFICATION

In this section a brief description of the failed coupling and its capability will be given based on the mechanical design of the coupling.

This coupling is one of the largest dry flexible type used in GE Oil & Gas application and, as already mentioned, connects the gas turbine to the first compressor of the LNG train in subject. (70 MW – 3600 rpm). Like all dry flexible couplings, it is composed by a rigid spacer (principal responsible of the realized torsional stiffness) and, at each spacer ends, 2 flex units designed to absorb axial thrusts from the machines and /or to adapt vertical and horizontal misalignment of the machines shafts. The flex units (2 double diaphragms in this case) are connected to the machines by a flange adaptor (failed part) to the turbine and by a taper hub to the compressor shaft.

The coupling capabilities are summarized in and are described below.

Table 1: DESIGN VERIFICATION DATA

Speed	Mean Torque	Axial	Bending	Cyclic Torque
(RPM)	(Nm)	(N)	(Nm)	(Nm)
3600	290578	34708	1313	55000

The light green cells in the table are the steady components of stress. The yellow ones contain the cyclic components. We have:

- Speed: it is the 100% of the coupling speed. It gives a centrifugal field of stress on all the components

- Mean Torque: it is the maximum continuous torque that the coupling is designed to transmit in combination to all the other loads
- Axial: it is the maximum axial load (consequence of an axial compression or tension) that the coupling is designed to transmit in combination to all the other loads
- Bending: it is the maximum bending moment (consequence of a shaft misalignment) that the coupling is designed to transmit in combination to all the other loads
- Cyclic Torque: it is the maximum 0-Pk cyclic torque that the coupling is designed to transmit in combination to all the other loads.

The coupling capability was verified in the failed point using a FE analysis and a fatigue assessment by Goodman diagram. All the load cases were singularly run and the mean stresses and the cyclic stresses were put all together in 2 separate load case combinations. The FEM results are shown at , , and .

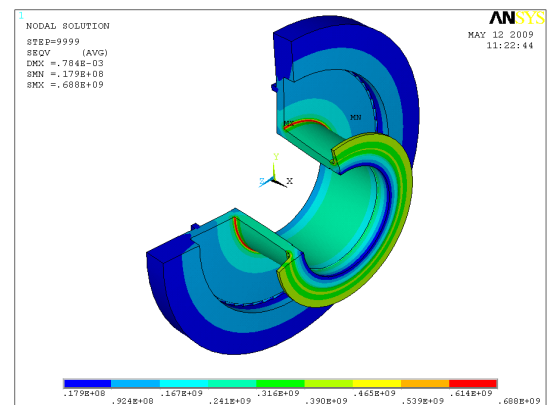


Figure 9: OVERALL VON MISES MEAN STRESS CONTOUR PLOT

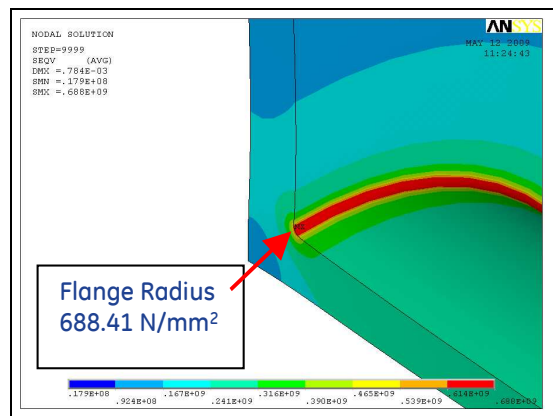


Figure 10: CLOSE UP VON MISES MEAN STRESS CONTOUR PLOT

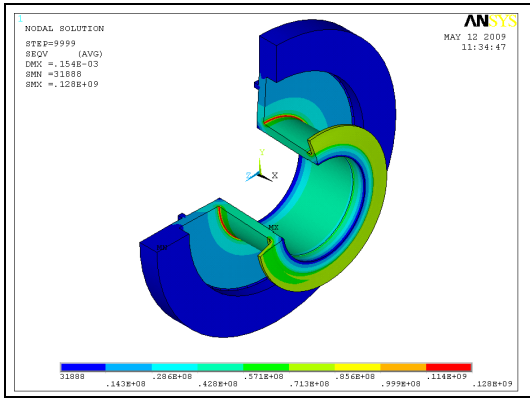


Figure 11: OVERALL VON MISES CYCLIC STRESS CONTOUR PLOT

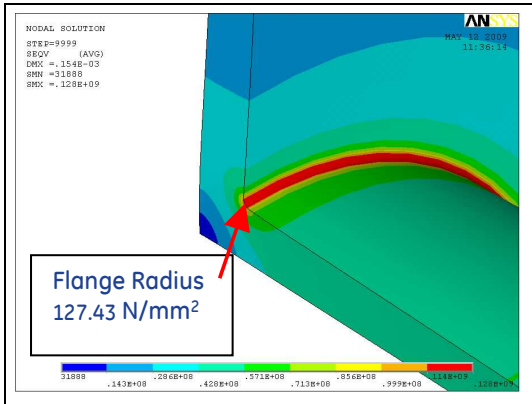


Figure 12: CLOSE UP VON MISES CYCLIC STRESS CONTOUR PLOT

The resulting Goodman diagram is shown at the figure. The red line is the modified Goodman infinite life (obtained from Wöhler tests with high cycles fatigue resistance $>10^7$ cycles) and the blue line is the life safety factor (1.18) obtained during design verification. The knee at the lower right end of the figure is a characteristic correction used to take in account the yield strength of the material.

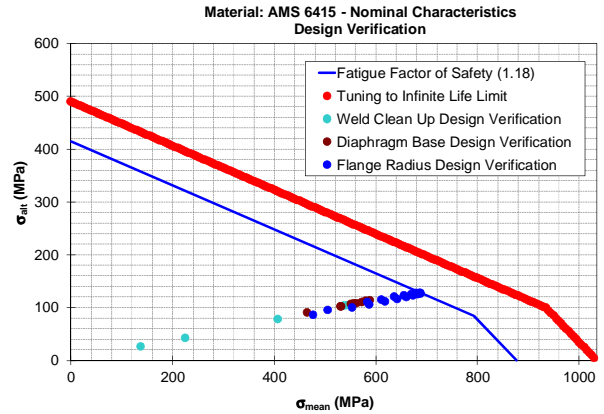


Figure 13: DESIGN VERIFICATION GOODMAN DIAGRAM

The conclusion is that the peak stress in the flange adapter with all applied loads has a 1.18 service factor on the infinite life limit (red line). Therefore as designed the coupling stress results are suitable for the application. It must be considered that the real operating conditions are much less severe than what considered in terms of coupling capabilities. The mean torque is not higher than 198000 Nm and the bending and axial stresses should be normally negligible. The cyclic torque is in general much lower than 55000 Nm. With this being said, there must be an additional stress riser or operational impact that then occurs for the failure to occur.

4. MATERIAL VERIFICATION

In order to understand the failure, a test campaign able to characterize the material and the manufacturing process was implemented. In are reported the chemical composition of the analyzed samples and the specification requirements.

Table 2: CHEMICAL COMPOSITION

		Elements									
		C	Mn	Si	P	S	Cr	Ni	Mo	Cu	Al
AMS 6415P	Max	0.43	0.85	0.35	0.025	0.025	0.90	2.00	0.30	0.35	-
	Min	0.38	0.65	0.15	-	-	0.70	1.65	0.20	-	-
Coupling		0.41	0.83	0.30	0.018	0.014	0.85	1.69	0.26	0.18	-

Macrostructure etching allows highlighting the grain structure and forging fiber orientation, with focus on detecting as close to fillet radius area the fiber moving from axial to perpendicular orientation.

Related to these findings, a tensile test campaign was conducted in order to check influence of the forged fiber orientation on material strength in the relation to the cracked area of the coupling. An image of the fracture surface of the tensile sample after test shown in



Figure 14: BRITTLE SURFACE OF TENSILE SAMPLE

This tensile tests are generally consistent with the material specification requirements except for the low ductility values that should be connected with different fiber orientation in different zones of the component (that lead the elongation to have very low values). The figure shows the brittle appearance of the final failure, consistent in brittle behaviors of the material, in particular in the flange radius area. In are resumed the required and the obtained tensile characteristics.

Table 3: RESULTS OF THE TENSILE TESTS

	Tensile Strength	Yield Strength	Elongation
	[Mpa]	[Mpa]	[%]
AMS 6415P	1172	1034	10
Coupling	1248	1117	9

A fatigue testing campaign was performed to estimate the infinite life fatigue limit of the material in the failed location. The tests were performed on an identical piece taken from another coupling adapter machined using the same material and the same forging and manufacturing processes. Samples have been taken from the same position where the failure occurred in the investigated component. Fatigue testing was conducted at room temperature in load control on servo-hydraulic equipment employing a 30 Hz sinusoidal waveform and an R ratio of -1. The results showed a 32% strength reduction due to the manufacturing process. An as-measured Goodman diagram based on the reduced material characteristics has been reported in in order to check the reliability of the component under design and normal operating conditions. In the graph, the blue point is characteristic of the design verification (worst condition); the black point is, instead, the expected stress working point of the coupling, obtained considering the normal cyclic torque and the mean torque during normal power generation (about 75 MW).

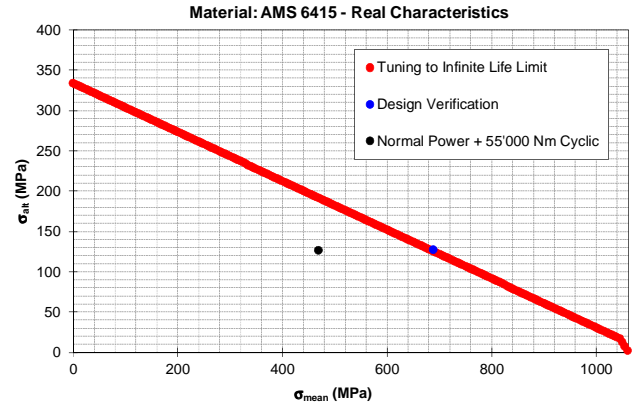


Figure 15: GOODMAN DIAGRAM WITH REDUCED MATERIAL CHARACTERISTICS

As can be seen, rated mean torque (290578 Nm, design verification) and normal mean torque (198000 Nm, normal power condition) combined with the guaranteed cyclic torque (55000 Nm) are not sufficient to drive the coupling to a failure.

5. MEASUREMENTS OF ALTERNATING TORQUE

Since an abnormal level of cyclic torque was considered to be a potential cause of the coupling damage, a site torsional vibration test was scheduled and carried out using the standard instrumentation installed on the train: speed pick-up and turbine/compressor phase mark).

Alternating torque was estimated starting from the measurement of speed oscillation at turbine suction side.

This methodology relies also on modal representation of dynamic system and was validated against test data coming from several LNG production train measurement campaigns, where the alternating torque was also directly measured by means of standard additional instrumentation (strain gauges).

Scope of the test was to check cyclic torque at full speed (3600 rpm) with different helper motor loads.

Three different test campaigns were all in all carried at site:

1. First Campaign to measure torsional vibration (TV) during train normal operation;
2. Long Term monitoring to keep under control the phenomenon during production phases;
3. Final Campaign to test/validate the implemented solution.

The following discussion focuses on the first test campaign in which torsional vibration values above the acceptable limit were detected.

provides an overview of the DAS Layout.

A single data acquisition system:

- 50 kHz;
- 32 Ch Simultaneous Sampling

was used to collect in parallel:

- Electrical Measurements;
- Torsional Vibration Measurements;
- GT Control System Data.

In particular TV data are collected from speed pick up, phase mark #1 and phase mark #2 (see).

In order to investigate the influence of the HM on this phenomenon, it was tested raising the load from 1 to 14 MW. It was noted that until the load remained below 11 MW the level of TV was almost steady with values within acceptable limit. The situation changed when overcoming 12 MW becoming finally dangerous at 14 MW where TV reached 1.1° of angular oscillation.

reports Coupling Twist Angle and Alternating Torque values at different HM load.

gives a screenshot of TV FFT analysis at 14 MW HM load: the 1st TNF component is clearly visible.

Table 4: ALTERNATING TORQUE VS HM LOAD

HM Load [MW]	Twist Angle [deg 0-pk]	Alternating Torque [KNm 0-pk]
14	1.12	112
12	0.44	44
1-11	0.30	30

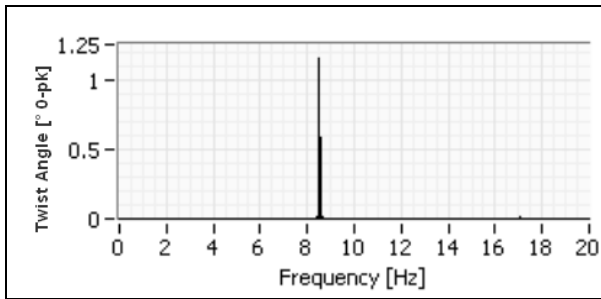


Figure 16: FFT OF TV AT 14 MW HM LOAD

Values listed in are calculated starting from the shaft modal shape monitoring the instantaneous speed oscillations at GT suction side as explained below.

1. Shaft “i” Revolution time (dt_i) monitored through Key Phasor signal (see);
2. Revolution-to-revolution time change allow to calculate shaft speed oscillation: $(dt_i \neq dt_{i+1} \neq dt_{i+n}) \Rightarrow d\omega(t)$

3. Angular oscillation at turbine suction site $\alpha(t)$ is calculated as the integral of the speed oscillation:

$$\alpha(t) = \int d\omega(t) dt$$

4. Given the angular oscillation “ α ” coupling twist angle “ β ” is evaluated through train mode shape (see)

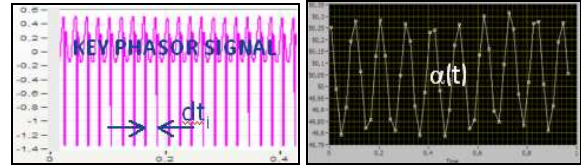


Figure 17: DETECTED SPEED OSCILLATIONS

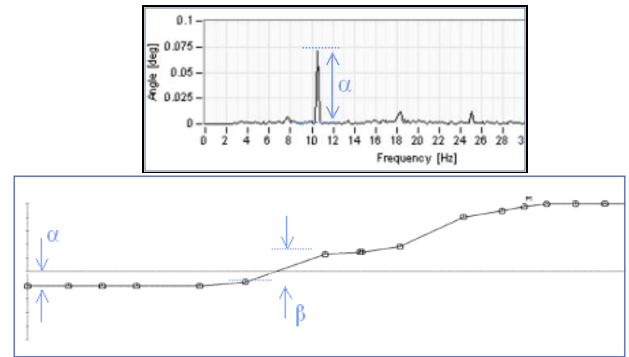


Figure 18: STRESS EVALUATED STARTING FROM MODE SHAPE

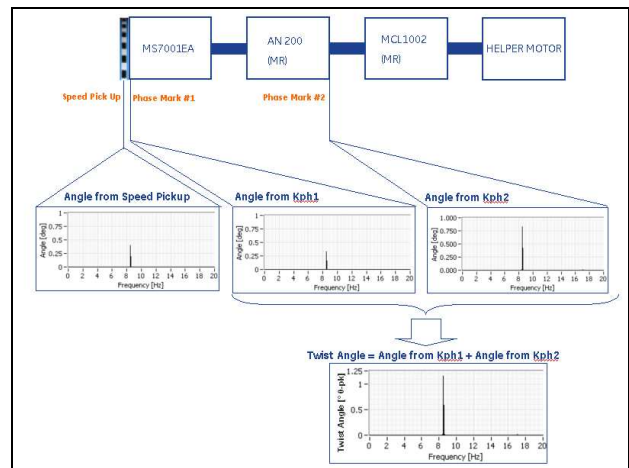


Figure 19: INSTRUMENT SIGNAL FFT

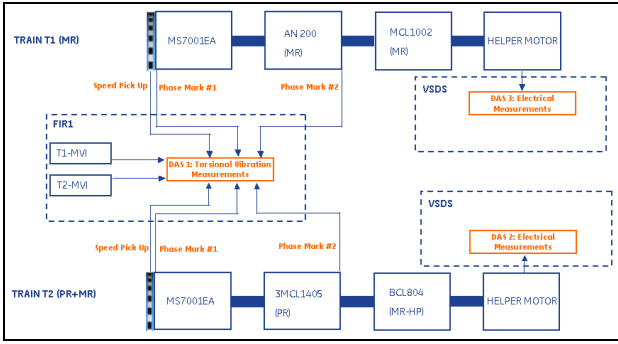


Figure 20: DATA ACQUISITION SYSTEM LAYOUT

In conclusion of this test campaign was understood that:

- TV amplitude was directly affected by HM load;
- Alternating Torque was above the acceptable limit.

The hypothesis of high TV as a root cause was then reinforced by the test measurements at site, as alternating torque values up to 112 kNm 0-pk were detected.

6. FRACTURE MECHANIC ASSESSMENT

A failure analysis is a process that can be approached in many different way but a reliable understanding of what happened and why it happened requires the input of a competent materials engineer joined with structural or design engineer.

Leveraging the information obtained by fractographic examination (fatigue striation density), a fracture analysis can be performed. In this phase FE (finite elements) simulation and fracture mechanic calculations are used in combination in order to characterize the stress condition on the component.

Using FE software is possible to perform a simulation to estimate the stress on the component based on the applied loads. Combining design and field data it is possible to accurately obtain an accurate applied stress and strain on the component.

Fracture mechanics approach (using British R6 method [8]) has been adopted in order to estimate the alternate stresses (and the torques) that promoted crack origin and crack propagation in the flange radius area.

This approach was based on fatigue striations counts performed by SEM analysis of several regions of the fracture surface as described in chapter 0.

The FE simulations performed have been used to define the membrane and bending static stresses on the component.

In the graphs shown in (as an example), is plotted Δl ($\mu\text{m}/\text{cycle}$) vs l (mm) direction; the red points in the graphs represents the zone where fatigue striations have been counted (by using of SEM).

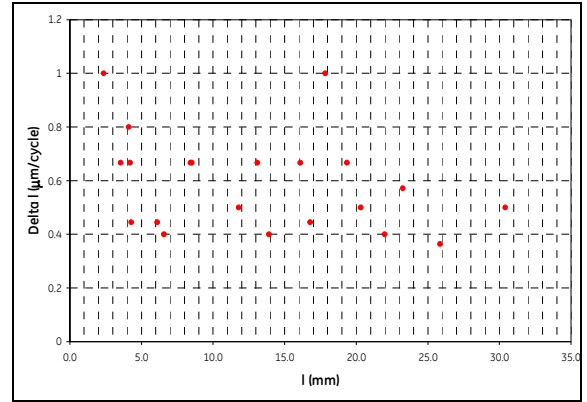


Figure 21: STRIATION DENSITY IN "L" PROPAGATION DIRECTION

For different regions of the fracture surface (like shown in), there are calculated stresses and torques necessary to have propagation in accordance with the counted fatigue striations. These calculations are performed using an internal tool, based on British R6 formulas that take in account the different geometric parameters used to calculate the ΔK during propagation of the crack (stress are constant during propagation, in accordance with the code). This value determines the real alternating load acting on the component.

As can be seen, this distribution of striation/micron is very different in respect with expected trend. In this case, there is a higher variability of distribution, different depending on the analyzed area. This is a clear index of the different stresses acting on the component during crack propagation.

Plotting the torque values that can promote crack propagation in the various analyzed points (the red points in), is simple to verify that this parameter has an "oscillating" trend but it decreases with the distance from the crack origin (lower stress need to crack propagation with bigger defect). It is very important to pay attention that the "rough" zones are characterized by higher value of the stresses during propagation (in the graph, the peak are relative to the rough zones). In the trend of torque vs crack propagation is shown.

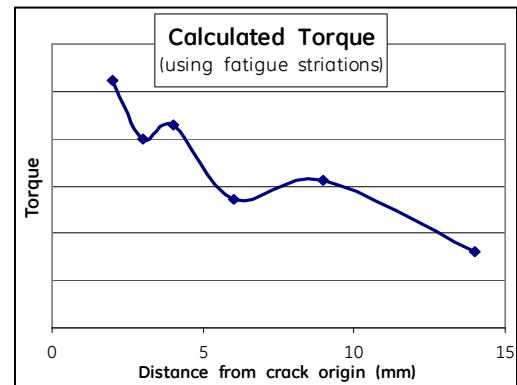


Figure 22: TORQUE VS CRACK PROPAGATION

7. FINAL ASSESSMENT

Finally, using the cyclic torques calculated by the fracture mechanics and confirmed by the torsional measurements, and considering the real material fatigue characteristics, we obtained a multitude of potential operative points on the Goodman diagram above the infinite life range, demonstrating the potential weakness of the failed part longevity on the mentioned operative conditions.

The final Goodman diagram is shown in the here below. The tables embedded in the graph explain the different analyzed points (identified by different static and cyclic loads).

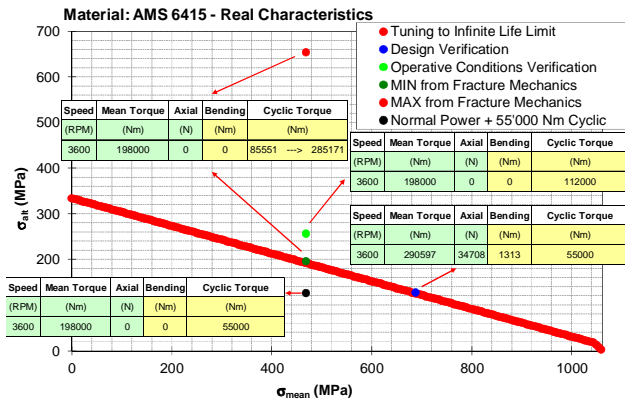


Figure 23: SUMMARY GOODMAN DIAGRAM

8. CONCLUSIONS

The most significant root cause proven in this investigation is suboptimal forging fiber orientation, which makes the finished piece less deformable than expected and below specifications, especially close to the failed flange radius. The yield stress and the tensile strength are inside the specific requirements wherever the specimen is taken. On the other hand the fatigue test revealed that the infinite life fatigue limit of the material is 334 MPa instead the nominal value 490 MPa (32% below expectations).

The measurement campaign carried out showed for short operational periods where cyclic torque is very high (112000 Nm). This torque, combined with a normal steady torque of 198000 Nm (74650 KW) is sufficient to drive the coupling to a fatigue failure in the flange radius location – combined with the fact the infinite life fatigue limit of the material is 334 MPa instead the nominal value 490 MPa (32% less).

The fractographic examination gave many pieces of information on the crack growth. It was possible to distinguish different load conditions experienced by the coupling in terms of cyclic stress (smooth and rough crack path). The final result was the different alternating stresses experienced during the crack propagation and the relevant torques correlated to these

stresses by FEM. When high cyclic torques was detected (by field measurements), in most the cases, it was larger than that initially measured and always larger than the allowable one (55000 Nm) original expected in the design. All these torques, combined with a normal torque of 198000 Nm (74650 KW) are sufficient to drive the coupling to a fatigue failure in the flange radius location.

The fatigue life assessment performed using the cyclic torque values demonstrates that the coupling, before the crack propagation, has suffered “consuming life” conditions. Since the infinite life limit is overcome with the measured operational conditions, it must have had a main role in the crack initiation, especially in the case of decreased fatigue life material limit.

The rated mean torque (290578 Nm) and normal torque (198000 Nm) combined with the guaranteed cyclic torque (55000 Nm) are not enough to drive the coupling to a failure without the reduction of the infinite life fatigue limit of the material of 334 MPa instead of the nominal value of 490 MPa (32% below expectations). With the material fatigue life at the minimum properties of the specification, the factors of safety are FoS = 1 for the rated torque and FoS = 1.27 for the normal torque.

NOMENCLATURE

AC	Axial Compressor
CC	Centrifugal Compressor
EHS	Environment, Health and Safety
FFT	Fast Fourier Transformation
FCG	Fatigue Crack Growth
FE	Finite Element
GT	Gas Turbine
HM	Helper Motor
LNG	Liquefied Natural Gas
MR	Mixed Refrigerant
PR	Propane
RCA	Root Cause Analysis
SEM	Scanning Electron Microscope
TV	Torsional Vibration

REFERENCES

- [1] Viggiano F., Schmied J., “Torsional instability of a geared compressor shaft train”, ImechE 1996.
- [2] Masayuki K., Takeshi H., Yasunori T. (2007) “Study of rotordynamic analysis method that considers torsional and lateral coupled vibrations in compressor trains with a gearbox”, Proceedings of the 36th Turbomachinery Symposium, Texas A&M University, Texas.
- [3] Perera I. “Theoretical and Experimental Study of Coupled Torsional-Lateral Vibrations in Rotor Dynamics”, University of Calgary, Thesis 1998

- [4] Iida H., Tamura A., & Yamada Y., (1978) "Coupled Torsional-Lateral Vibration of Shaft in a Geared Rotor System I", Bulletin of JSME, Vol23, No186, December 1980.
- [5] Iida H., Tamura A., & Oonishi, M., (1984) "Coupled Torsional-Lateral Vibration of Shaft in a Geared Rotor System II", Bulletin of JSME, Vol28, No245, December 1985.
- [6] Wachel J.C., & Szenasi F.R., (1980) "Field Verification of Lateral-Torsional Coupling Effects on Rotor Instabilities in Centrifugal Compressors", NASA Conference Publication No. 2147, 1980.
- [7] Castellini, P. and Santolini, C., (1998), "Vibration Measurement on Blades of a Naval Propeller Rotating in Water with Tracking Laser Vibrometer", Measurement, Vol. 24, 43-54
- [8] BS 7910:2005, "Guide to Methods for Assessing the Acceptability of Flaws in Metallic Structures", BSi, 2005.
- [7] Castellini, P. and Santolini, C., (1998), "Vibration Measurement on Blades of a Naval Propeller Rotating in Water with Tracking Laser Vibrometer", Measurement, Vol. 24, 43-54
- [8] BS 7910:2005, "Guide to Methods for Assessing the Acceptability of Flaws in Metallic Structures", BSi, 2005.